Supporting information

Large Area Nanofabrication of Partially Embedded Nanostructures for Enhanced Plasmonic Hot Carrier Extraction

Charlene Ng,[*,†,Ψ] Peng Zeng,[‡] Julian A. Lloyd,[¶] Debadi Chakraborty,[§] Ann Roberts,[∥] Trevor A. Smith,[‡,⊥] Udo Bach,[¶,⊥] John E. Sader,[§,⊥] Timothy J. Davis,[∥] Daniel E. Gómez[*,#,†,⊥]

†CSIRO, Manufacturing, Private Bag 33, Clayton, VIC, 3168, Australia

‡School of Chemistry, The University of Melbourne, VIC 3010, Australia

¶Department of Materials Science and Engineering, Monash University, Clayton, VIC 3800, Australia

§School of Mathematics and Statistics, The University of Melbourne, VIC 3010, Australia ∥School of Physics, The University of Melbourne, VIC 3010, Australia

⊥ARC Centre of Excellence in Exciton Science

#RMIT University, Melbourne, VIC, 3000, Australia

[Ψ] Current Address: Leibniz Institute for Polymer Research, 01069 Dresden, Germany

Appendix S1: Au nanorods and AFM cross-section

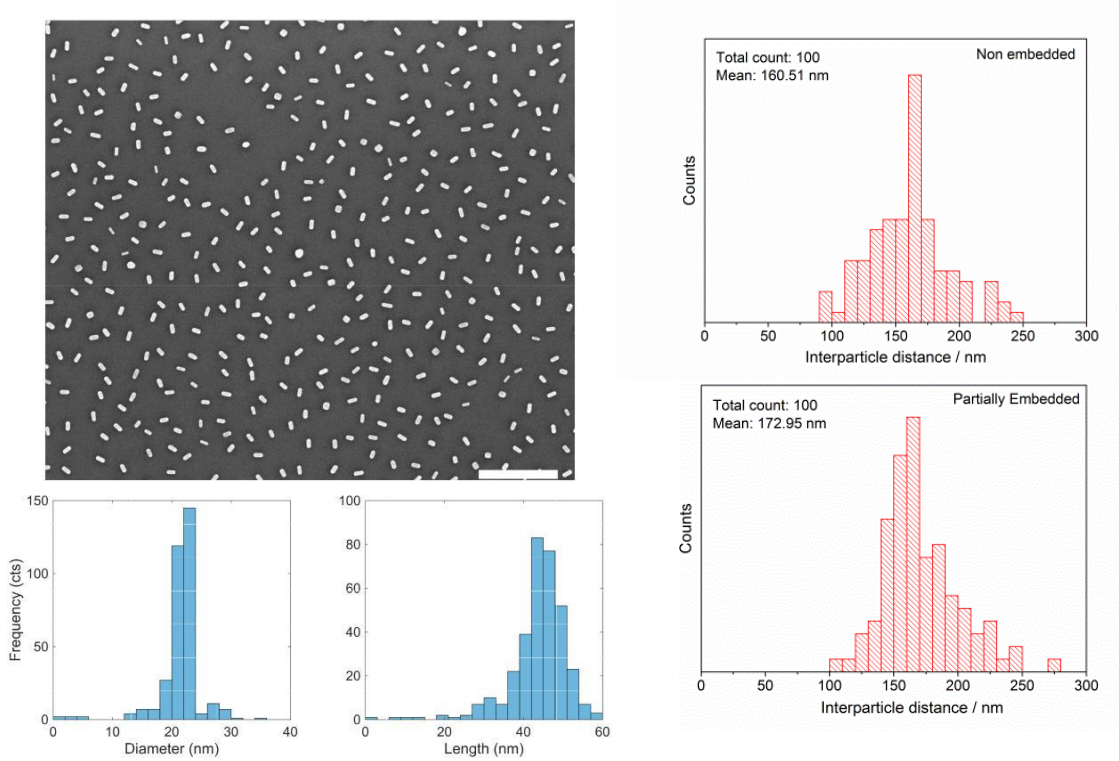

FIG. S1: **Au nanorods.** (top) SEM micrograph of a typical Au-nanorod assembly on a glass substrate. Some impurities such as spherical nanoparticles or Au-nanorods with a different size or aspect ratio are visible.(Scale bar: 500 nm). (bottom). Histograms of the (left) diameter and the (right) length of the nanorods. Right: Histogram of interparticle distance of embedded and nonembedded structures.

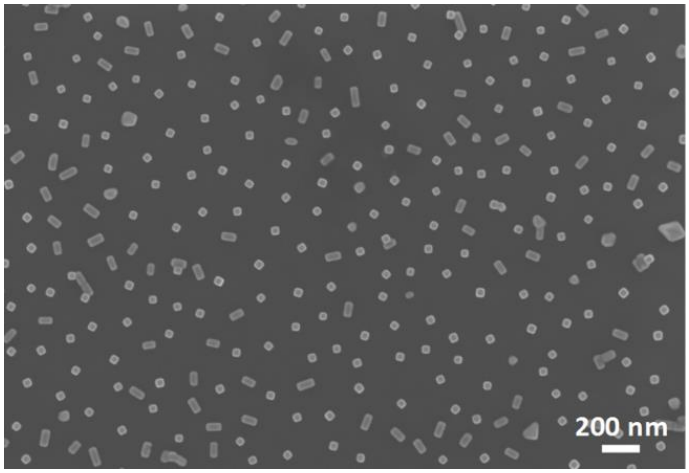

FIG S2: TMAC coated Silver cuboids deposition onto MMA supported by Si wafer to demonstrate the flexibility of the introduced fabrication method.

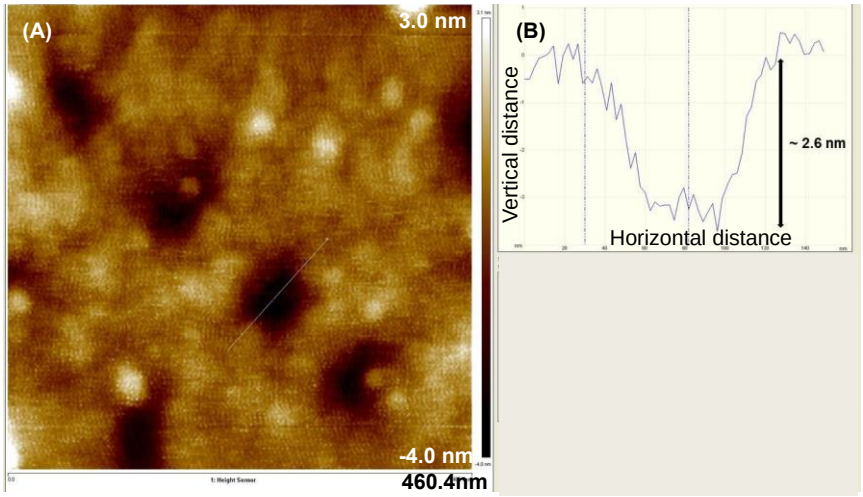

FIG. S3: **Cross-sectional AFM image.** The cross-sectional dimensions of the embedded structures from AFM imaging to confirm that the Au nanorods are buried 2 nm below the TiO_2 surface, where (A) is the AFM image and (B) is the measured depth over a section of the embedded structure.

Appendix S2: Mirror-semiconductor-nanorod structures

Here we present the experiment results obtained when creating metal-semiconductor-metal structures. These structures were fabricated as described in Figure 2 of the main text except for the inclusion of an aluminium (Al) mirror (200 nm thickness), which was sputtered on top of the TiO_2 prior to MMA lift-off , as indicated in figure S3.

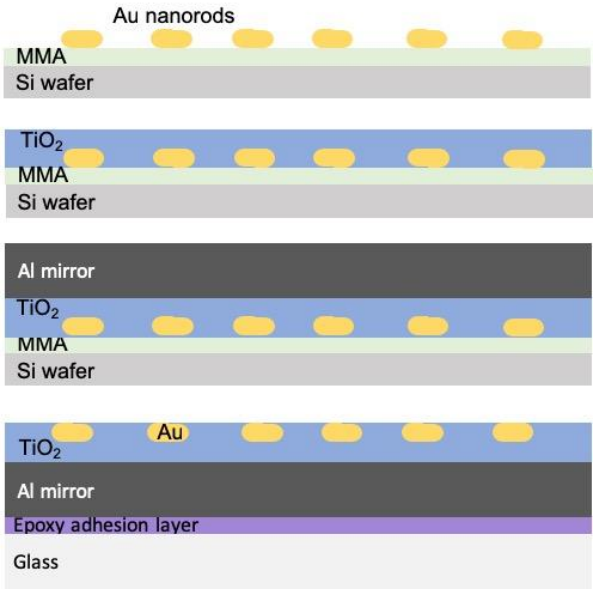

Figure S4: Fabrication of the structure with the additional of a metal mirror.

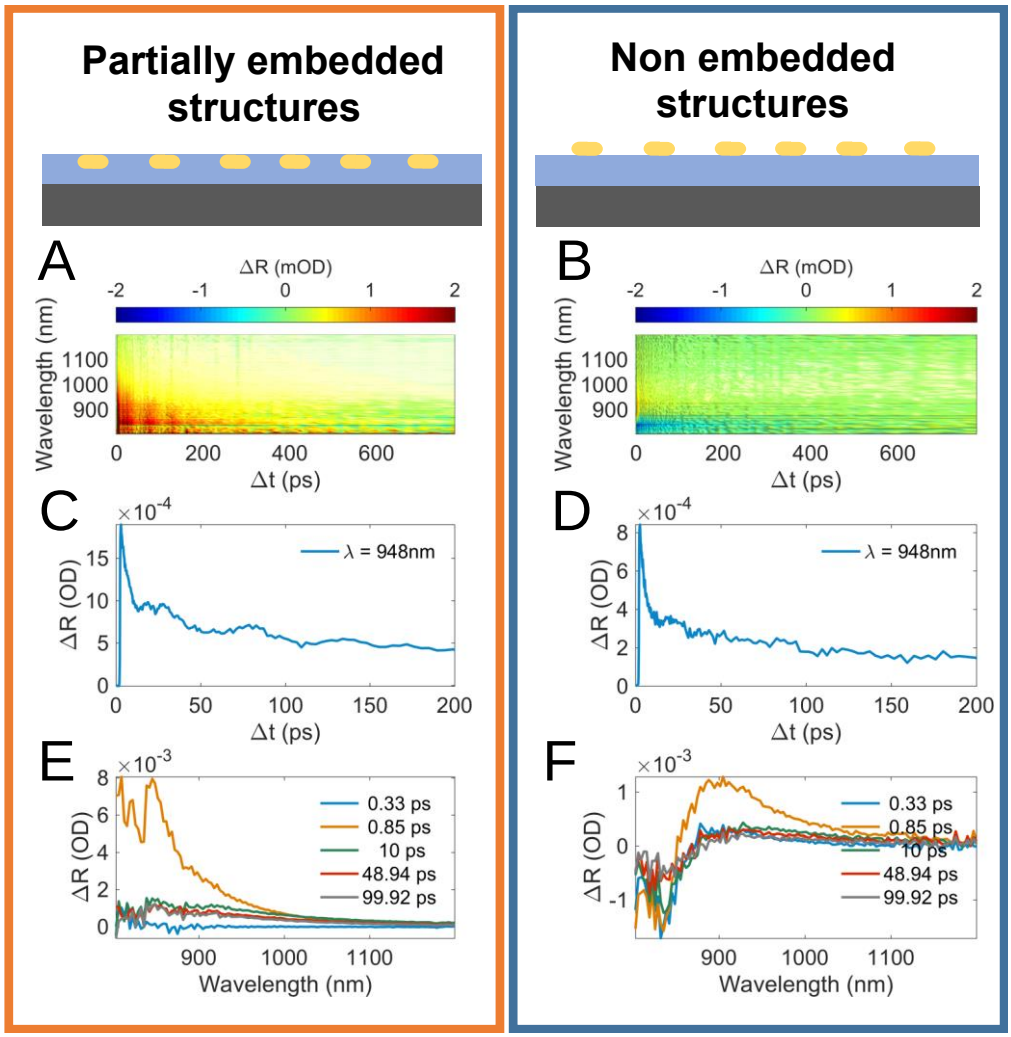

FIG. S5: **Ultra-fast pump probe spectroscopy.** (A) and (B) show the difference reflectance spectra as a function of wavelength and pump-probe delay time (Δt) for the partially and non-embedded structures respectively. (C) and (D) show the time evolution of the differential reflectance spectrum probed at a wavelength of approx 840 nm. (E) and (F) show differential spectra as function of probe wavelength for different pump-probe delay times. In both cases λ_{pump}: 634 nm at a fixed incident fluence of 3.5×10^{-5} W/cm^2.

Figure S5 shows the results of transient pump-probe measurements performed in reflectance mode, for metal-semiconductor-nanorod samples where the nanostructures are partially embedded and deposited on top of thesemiconductor. As mentioned in the main text, panel S5A shows clear evidence of damped oscillations in the measured signals, which we ascribe to mechanical oscillations of the nanorods.

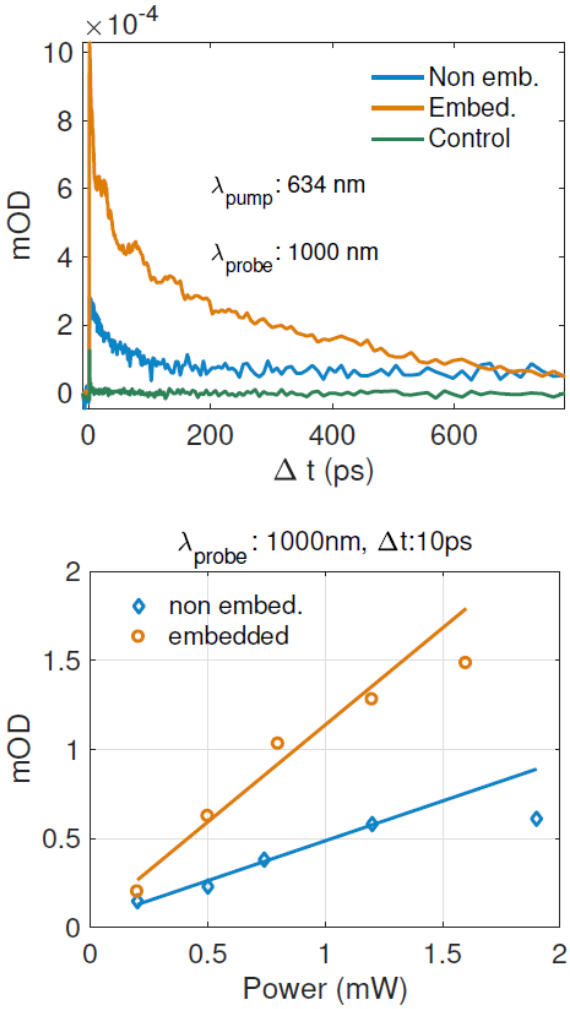

FIG. S6: **Pump-Probe comparison.** (Top) Time evolution of the differential reflectance signal measured at 1000 nm for samples consisting of Au nanorods on glass, on TiO_2 and partially-embedded in TiO_2. In all three cases the experiment conditions were kept fixed. (Bottom) Measured intensity of the transient reflectance signal vs incident pump power for the embedded and non-embedded samples with fitted lines.

Figure S6(Top) shows a comparison of the amplitude of the measured signal, similar to the one made in figure 5A of the main text. Figure S6 (Bottom) shows the measured power-dependence of the transient signal for the embedded and non-embedded samples, along with linear fits. The slopes of these fits are 0.45 mOD/mW for the non-embedded structures and 1.09 mOD/mW for the embedded ones (roughly a factor of ~2.4 greater).

Appendix S3: Assignment of mechanical oscillations

We now consider the vibrational modes of a gold nanorod embedded in TiO_2. Figure S7(A) shows the cross section of the examined system. Given that the mechanical coupling strength of the Au-TiO_2 interface is unknown, finite element simulations were carried out assuming the existence of a very thin layer of an artificial material with variable stiffness between the Au nanorod and the substrate. When the stiffness of the thin layer is small, the substrate does not influence the nanorod motion. However, with increasing stiffness, the substrate restrains the mechanical oscillations of the nanorod. The simulations predict a dominant breathing mode vibration at 22.5 GHz for weak mechanical coupling with the TiO_2 substrate. This vibration mode originates due to the deformation along the width [see Figure S7(B)]. For a stronger binding strength with the TiO_2 layer, the dominant oscillation frequency can reach up to 40.8 GHz. Experimental results shown in figure S7C and D indicate a vibrational frequency of 20 GHz which suggests a weak mechanical interaction between gold nanorods and TiO_2 at the interface.

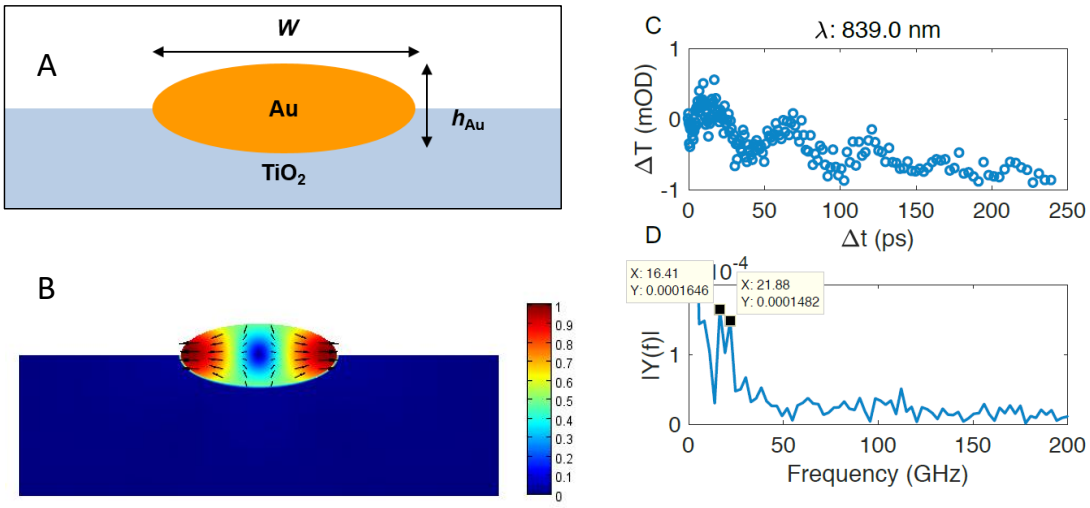

FIG. S7: **FEM mechanical model.** (A) Schematic of the embedded nanorod geometry that is modeled. (B) FEM simulations of the acoustic vibration mode of single Au nanorod embedded in titanium dioxide. A cross-sectional view of the nanorod is presented, where arrows indicate the direction of the displacement field. The colour scale bar represents the normalized displacement field (C) Evolution of the measured transient signal of figure S5A at a probe wavelength of 839 nm showing damped oscillations. D. Fourier transform of the data of panel C.

Appendix S5: Pump-probe spectroscopy: Further experiment details

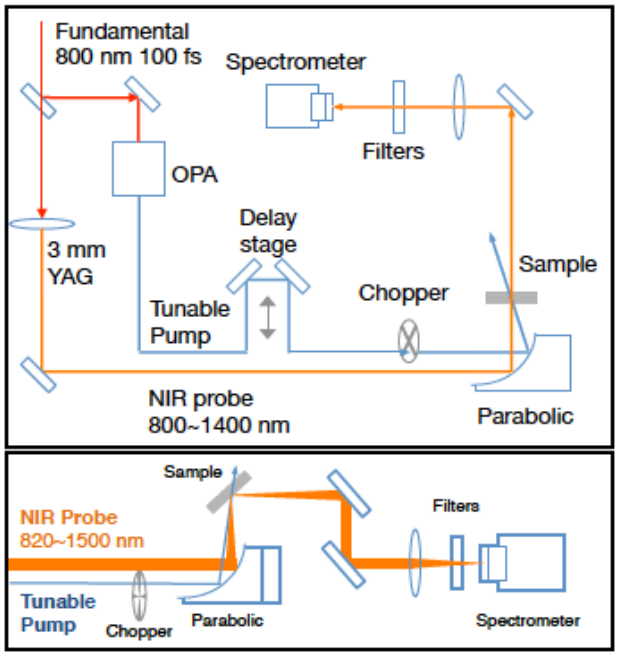

FIG. S8: **Pump-probe configuration** (Top) transient absorption and (Bottom) transient reflectance measurements.

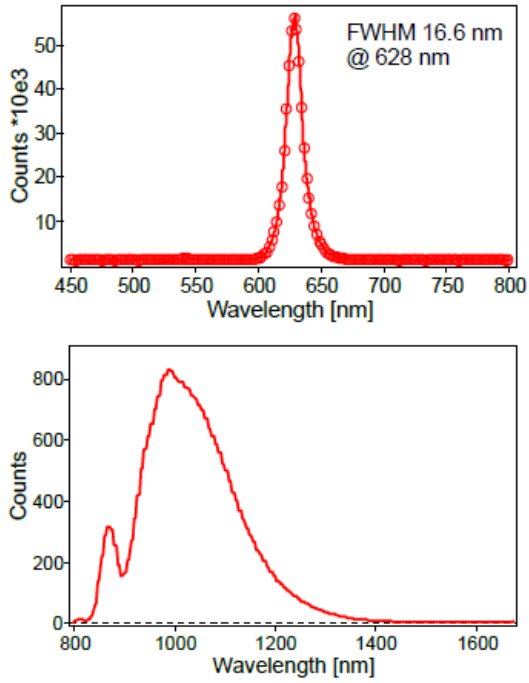

FIG. S9: **Spectra of (top) pump and (bottom) probe light.** For the probe we show one of the central wavelengths. Similar spectral lineshapes are obtained at other spectral positions. The measured spectral bandwidth of the pump (FWHM) is around 17 nm at the wavelength of 628 nm. The output pulse from the OPA has a spectral bandwidth less than 20 nm for most wavelengths in the visible range.

For the transient absorption measurements, the excitation is nearly normally incident; the error in the angle of

incidence is less than 1 degree. The angular spread of the excitation is less than 2 degrees [$\sin^{-1}$(5mm/150mm)], where 5mm is the laser spot diameter before focusing, and the focal length of parabolic mirror is 150 mm.

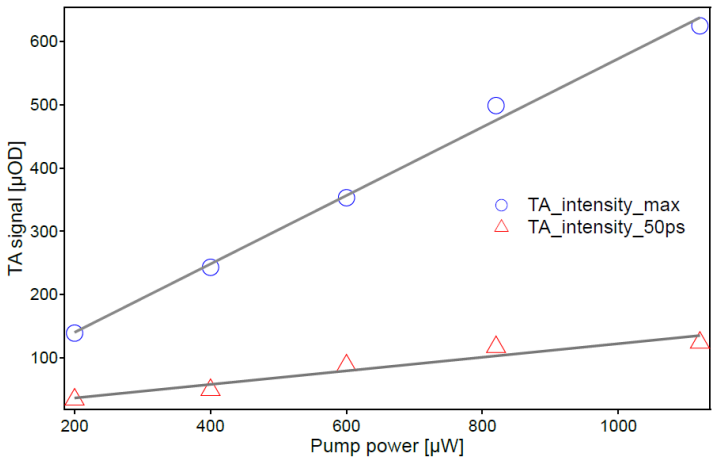

FIG. S10: **Pump-power dependence** of the transient absorption signal of Figure 4 of the main text at two different pump-probe delay times

Appendix S6: Experimental Methods

S6.1.Electromagnetic simulations

The absorption spectra of the Au nanorods were simu-lated via the Finite Element Method as implemented in COMSOL Multiphysics version 5.1, using the wave optics module. The total field was calculated in two steps. Firstly, the background field in the absence of the parti-cle was computed assuming periodic boundary conditions on the sides and ports at the plane wave excitation and transmission boundaries. This simulated an in finite domain. The result was then used as the background field in the calculation of the scattered field in the presence of a single particle. In this second calculation, the physical domain was chosen to have a rectangular geometry and was surrounded by perfectly matched layers on all sides to absorb the scattered radiation. The absorption in the particle was calculated by integrating the electromagnetic dissipation density over the volume of the particle. The rate of electron injection was calculated as being proportional to the integral of the square of the magnitude of the electric eld over the fraction of the surface of the particle embedded in the TiO_2. The opti-cal properties of (bulk) gold were taken from Rakic et al. [4]

S6.2.Au-nanorod preparation

The gold nanorods used throughout the experiments were synthesised as presented by Thai et al. [5]. The as-synthesized Au-nanorods are coated with a bilayer of the cationic surfactant Cetyltrimethylammonium bromide (CTAB, Sigma Aldrich) which has to be replaced by a N,N,N-trimethyl-(11-mercaptoundecyl)ammonium chloride (TMAC, ProChimia) coating. 0.1 ml of the CTAB Au-nanorod solution are then diluted to 1 ml with MilliQ water and re-concentrated to 0.1 ml by centrifu-gation (1800 rcf, 40 min). After adding 8 µl 24 mM TMAC, the solution is left to incubate overnight. Excess CTAB and TMAC is removed from the solution by 4 sub-sequent washing cycles: the solution is refilled 1 ml with MilliQ water, centrifuged to precipitate the Au-nanorods at the bottom, 0.9 ml of solvent are extracted and the Au-nanorods re-dispersed by vortexing. A typical optical absorption spectrum of the resulting colloid is shown in Figure 3E. The colloid is diluted to optical density 1 (measured at the 637 nm wavelength) for the assembly.

S6.3.Au nanorod surface assembly

To self-assemble the Au-nanorods on a glass or MMA coated substrate, the substrate is immersed in the colloid for 3 h. The assembly process itself is based on electrostatic interactions: The TMAC-Au-nanorods carry a positive surface charge and adsorb readily on the substrate (which has a negative zeta-potential when immersed in the assembly solution). Due to repulsive interactions between the individual Au-nanorods they assemble with a uniform nearest-

neighbour distance (Figure S1). After assembly, the substrates are dip-washed (3 times) in MilliQ water and left to dry on air. Nanofabrication and characterization after the Au nanorods are assembled onto the MMA coated Si sub-strate, 50 nm of TiO_2 are deposited onto the surface via electron beam evaporation (Intlvac Nanochrome II electron beam evaporation system) at room temperature.

with a deposition rate of 1.0 A/s. For samples with an Al mirror (supporting information), 200 nm of Al are sputtered on top of the TiO_2 layer via a DC Sputtering system (Intlvac Nanochrome AC/DC system) at 100 W under Argon flow. Epoxy glue is then used to adhere the TiO_2 layer (for samples without Al mirror) or Al mirror to a glass substrate and the sample is left overnight to dry. Next, the sample is immersed in acetone (Sigma-Aldrich >99.5%) for 3 h to remove the MMA layer and release the final structure from the Si substrate. The final structure is then washed with Milli-Q water and left to dry in air before further characterization. For the non-embedded samples, the TiO_2 and Al layers are fabricated under same conditions described above in the absence of Au nanorods and the Au nanorods are later assembled onto the TiO_2 layer with and without an Al mirror under similar conditions. Scanning electron microscope (SEM) images of the surfaces were obtained with a FEI Field Emission Scanning Electron Microscope. The diffuse and specular reflectance (R) and transmittance (T) spectra were measured using a UV-VIS spectrophotometer (Perkin-Elmer Lambda 1050) with an integrating sphere and small spot kit.

S6.4.Ultra-fast pump-probe spectroscopy

Complete details of our experimental setup have been presented elsewhere [6]. A high-repetition-rate regenerative amplifier (Coherent RegA9050, 800 nm, 1 W, and 92 kHz) was employed as the laser source. The out-put pulses from the amplifier was compressed (Coherent EC9150) to 60 fs and later split into two branches for generation of pump and probe pulses. A branch of the output pumped a tunable optical parameter amplifier (Coherent OPA9450) to produce monochrome pump pulses (480{750 nm with FWHM less than 20 nm). Near-IR white light probe pulses (820-1500 nm) were generated by focusing the rest of fundamental pulses (800 nm) into a 3-mm-thick YAG window (CASTECH). A long-pass filter was used to block the fundamental and visible light in the probe pulses. Pump and probe pulses were focused on the sample with an o -axis parabolic mirror and overlapped at the sample surface with a pump spot size of 100 m in diameter. The pump pulses were incident on the sample at an angle of 34 while probe at an angle of 30 . The pump pulses were p-polarized with respect to the sample surface. The reflectance changes were measured by comparing adjacent probe pulses with and without pump pulses using a synchronized mechanical chopper in the path of the pump beam. The time-resolved transient reflectance spectra were recorded using an NIR high-speed fiber-optic spectrometer (Ultrafast System, 7100 spectra/ s, respectively). The delay time between pump and probe pulses was controlled using a motorized delay stage (Newport UTM-PP0.1, with step size of 0.66 fs and range of 800 ps). The temporal resolution of the whole setup was estimated at 200 fs (fwhm) by measuring the autocorrelation of fundamental pulses. A low noise level was achieved below $5x10^{-5}$ OD, by taking advantage of the high-repetition-rate laser and high signal averaging approach coupled with an acquisition process that rejected any outlying spectra. Photodegradation and thermal effects were avoided by using low incident powers, and their absence was ascertained by repeating the measurements several time ensuring identical outcomes.

[1] A. Furube, L. Du, K. Hara, R. Katoh, and M. Tachiya, Journal of the American Chemical Society 129, 14852 (2007)

[2] Y. Tian, X. Wang, D. Zhang, X. Shi, and S. Wang, Journal of Photochemistry and Photobiology A: Chemistry 199,
224 2008), ISSN 1010-6030

[3] A. V. Uskov, I. E. Protsenko, R. S. Ikhsanov, V. E. Babicheva, S. V. Zhukovsky, A. V. Lavrinenko, E. P. O'Reilly, and H. Xu, Nanoscale 6, 4716 (2014), URL .

[4] A. D. Rakic, A. B. Djurisic, J. M. Elazar, and M. L. Ma-jewski, Appl. Opt. 37, 5271 (1998), URL .

[5] T. Thai, Y. Zheng, S. H. Ng, S. Mudie, M. Altissimo, and
U. Bach, Angewandte Chemie International Edition 51, 8732 (2012), ISSN 1521-3773, URL .

[6] P. Zeng, J. Cadusch, D. Chakraborty, T. A. Smith, A. Roberts, J. Sader, T. Davis, and D. E. Gomez, Nano Letters 16, 2651 (2016)